THE JOURNAL OF BIOLOGICAL CHEMISTRY VOL. 282, NO. 51, pp. 37191–37204, December 21, 2007


# Crystal Structure of the Interleukin-15·Interleukin-15 Receptor α Complex

## *INSIGHTS INTO TRANS AND CIS PRESENTATION*[*] [S]

Received for publication, July 26, 2007, and in revised form, September 28, 2007 Published, JBC Papers in Press, October 18, 2007, DOI 10.1074/jbc.M706150200

**Shaun K. Olsen[‡], Naruhisa Ota[§], Seiichiro Kishishita[‡], Mutsuko Kukimoto-Niino[‡], Kazutaka Murayama[‡¶], Hidemi Uchiyama[§], Mitsutoshi Toyama[‡], Takaho Terada[‡], Mikako Shirouzu[‡], Osami Kanagawa[§], and Shigeyuki Yokoyama[‡‖1]**

*From the [‡]RIKEN Genomic Sciences Center and the [§]RIKEN Research Center for Allergy and Immunology, RIKEN Yokohama Institute, 1-7-22 Suehiro-cho, Tsurumi, Yokohama, Kanagawa 230-0045, the [¶]Tohoku University Biomedical Engineering Research Organization, Sendai 980-8575, and the [‖]Department of Biophysics and Biochemistry, University of Tokyo, Tokyo 113-0033, Japan*

**Interleukin (IL)-15 is a pleiotropic cytokine that plays a pivotal role in both innate and adaptive immunity. IL-15 is unique among cytokines due to its participation in a *trans* signaling mechanism in which IL-15 receptor α (IL-15Rα) from one subset of cells presents IL-15 to neighboring IL-2Rβ/$\gamma_c$-expressing cells. Here we present the crystal structure of IL-15 in complex with the sushi domain of IL-15Rα. The structure reveals that the α receptor-binding epitope of IL-15 adopts a unique conformation, which, together with amino acid substitutions, permits specific interactions with IL-15Rα that account for the exceptionally high affinity of the IL-15·IL-15Rα complex. Interestingly, analysis of the topology of IL-15 and IL-15Rα at the IL-15·IL-15Rα interface suggests that IL-15 should be capable of participating in a *cis* signaling mechanism similar to that of the related cytokine IL-2. Indeed, we present biochemical data demonstrating that IL-15 is capable of efficiently signaling in *cis* through IL-15Rα and IL-2Rβ/$\gamma_c$ expressed on the surface of a single cell. Based on our data we propose that *cis* presentation of IL-15 may be important in certain biological contexts and that flexibility of IL-15Rα permits IL-15 and its three receptor components to be assembled identically at the ligand-receptor interface whether IL-15 is presented in *cis* or *trans*. Finally, we have gained insights into IL-15·IL-15Rα·IL-2Rβ·$\gamma_c$ quaternary complex assembly through the use of molecular modeling.**

Interleukin (IL)[2]-15 is a member of the four-α-helix bundle family of cytokines, which plays a pivotal role in both innate and adaptive immunity (1, 2). IL-15 was initially identified due to its ability to mimic the activity of IL-2 *in vitro* (3, 4), and despite a lack of significant sequence homology, IL-15 and IL-2 are able to similarly stimulate the proliferation and differentiation of natural killer (NK), T, and B cells (1, 2). Despite these many overlapping functions, IL-15 and IL-2 possess distinct biological activities *in vivo*, such as the ability of IL-15 to control the development of $CD8^+$ memory T cells and the involvement of IL-2 in the maintenance of regulatory T cells (5).

The cell-surface receptor for IL-15 comprises three subunits: IL-15 receptor (IL-15R) α, IL-2Rβ (also known as IL-15Rβ, CD122, and p75), and $\gamma_c$ (also known as CD132 and p65). The ectodomain of IL-15Rα consists of a single sushi domain (6) (also known as a short consensus repeat or complement control protein repeat), which is essential for IL-15 binding and IL-15Rα function (7, 8), a membrane-proximal proline-threonine-rich (PT) region, and a linker/hinge region that connects the sushi domain and the PT region (6). IL-2Rα is structurally related to IL-15Rα but contains an additional sushi domain that is connected to the first by a linker region. The ectodomain of IL-2Rβ and $\gamma_c$ each consist of two fibronectin-type III domains, which participate in IL-15 binding (9), and the cytoplasmic domains of IL-2Rβ and $\gamma_c$ sequester signaling molecules such as Jak1 and Jak3 (10, 11). In contrast, the short cytoplasmic domains of IL-15Rα and IL-2Rα are not thought to play a major role in signaling (12), although the cytoplasmic domain of IL-15Rα has recently been shown to play a role in receptor recycling (13). Because IL-2Rβ and $\gamma_c$ are shared subunits of the receptor for IL-2 (6, 12, 14), IL-15 and IL-2 are capable of activating similar signaling pathways, including Jak1/Jak3 and Stat3/Stat5, Ras/mitogen-activated protein kinase, and phosphatidylinositol 3-kinase pathways (1), which has been suggested to partially account for the overlapping functions of IL-15 and IL-2.

A possible mechanism by which IL-15 and IL-2 attain their distinct *in vivo* functions is through differences in the properties of their α chain receptors. IL-15Rα binds specifically to IL-15 with high affinity ($K_d$ = 30–100 pM) (6, 12, 15, 16), whereas IL-2Rα specifically binds to IL-2 with a comparatively lower affinity ($K_d$ = 10–30 nM) (17). IL-15, IL-2, and their α chain receptors also exhibit distinct expression profiles, which have been suggested to contribute to their distinct biological

* This work was supported by the RIKEN Structural Genomics/Proteomics Initiative, the National Project on Protein Structural and Functional Analyses, Ministry of Education, Culture, Sports, Science and Technology of Japan. The costs of publication of this article were defrayed in part by the payment of page charges. This article must therefore be hereby marked "*advertisement*" in accordance with 18 U.S.C. Section 1734 solely to indicate this fact.

*The atomic coordinates and structure factors (code 2PSM) have been deposited in the Protein Data Bank, Research Collaboratory for Structural Bioinformatics, Rutgers University, New Brunswick, NJ (http://www.rcsb.org/).*

[S] The on-line version of this article (available at http://www.jbc.org) contains supplemental Figs. S1 and S2 and an additional reference.

[1] To whom correspondence should be addressed. Tel.: 81-45-503-9196; Fax: 81-45-503-9195; E-mail: yokoyama@biochem.s.u-tokyo.ac.jp.

[2] The abbreviations used are: IL, interleukin; R, receptor; MALDI-TOF, matrix-assisted laser desorption ionization time-of-flight; PT, proline-threonine-rich region; r.m.s.d., root mean square deviation.

activities (18). Furthermore, in contrast to IL-2, which acts as a soluble cytokine, IL-15 is coordinately expressed with IL-15Rα by activated monocytes and dendritic cells and is extremely difficult to detect in free form in humans and mice due to stable complex formation with IL-15Rα on the cell surface (13, 19–23). Recent data have demonstrated that IL-15Rα from activated monocytes presents IL-15 in *trans* to IL-2Rβ/$\gamma_c$ and/or IL-15Rα/IL-2Rβ/$\gamma_c$-expressing cells such as $CD8^+$ memory T cells and NK cells (13, 21, 24). This finding suggests that the architecture of IL-15R subunits in the IL-15 quaternary complex differs from that of IL-2 receptor subunits in the IL-2 quaternary complex, which are assembled in *cis* (*i.e.* on the surface of the same cell) as revealed by the recently reported IL-2·IL-2Rα·IL-2Rβ·$\gamma_c$ crystal structure (25, 26). Although *trans* presentation is currently thought to be the major mechanism by which IL-15 exerts its biological effects *in vivo*, the possibility for the assembly of a *cis* IL-15 quaternary complex on cells capable of expressing IL-15Rα, IL-2Rβ, and $\gamma_c$, has not been ruled out (18). However, considering the structural similarities between IL-15, IL-2, and their receptors (15, 27, 28), and data suggesting that IL-15 has only a single binding site for interaction with IL-15Rα (29), the molecular basis by which *trans* presentation occurs and can even co-exist with the formation of IL-2-like *cis* quaternary complex is not clear.

In this report, we present the crystal structure of murine IL-15 in complex with the sushi-domain fragment of IL-15Rα, refined to 2.2-Å resolution. The structure reveals the molecular determinants of the specific, high affinity IL-15·IL-15Rα interaction. Importantly, helix B and the hC–hD loop of IL-15 adopt unique conformations, which permit specific interactions with IL-15Rα that likely account for its significantly higher affinity relative to the IL-2·IL-2Rα interaction. We also present biochemical data demonstrating that, in addition to *trans* presentation, IL-15Rα is capable of presenting IL-15 to IL-2Rβ/$\gamma_c$ in *cis*, suggesting a potential role for *cis* IL-15 presentation in certain biological contexts. Finally, analysis of the structure suggests that flexibility of the linker and/or PT region of IL-15Rα permit IL-15 and its three receptor components to be assembled identically at the ligand-receptor interface whether IL-15 is presented in *cis* or *trans.*

## EXPERIMENTAL PROCEDURES

*Protein Expression and Purification*—The DNA fragments encoding the full-length ectodomain of mature murine IL-15Rα (residues 1–168; sIL-15R$\alpha^{1-168}$), and the full-length mature murine IL-15 (residues 1–114) were cloned into the TA vector pCR2.1TOPO (Invitrogen) as fusion proteins containing an N-terminal histidine tag and a tobacco etch virus protease cleavage site. Selenomethionine-labeled proteins were synthesized using the large scale dialysis mode of the *Escherichia coli* cell-free reaction (30). Both IL-15 and sIL-15R$\alpha^{1-168}$ precipitated during synthesis. The precipitated proteins were denatured in 25 mM Tris-HCl buffer (pH 8.3) containing 6 M guanidine hydrochloride and 1 mM dithiothreitol and were refolded separately or co-refolded by rapid dilution into 50 mM Tris buffer (pH 8.3) containing 1 M arginine hydrochloride, 5 mM reduced glutathione, and 0.5 mM oxidized glutathione. After stirring for 24 h at 4 °C, the protein solutions were filtered and dialyzed against 25 mM Tris-HCl buffer (pH 7.5) containing 150 mM NaCl for 12–24 h at 4 °C. The refolded proteins were purified to homogeneity by chromatography on affinity (HisTrap) and gel-filtration (Superdex 200 HR 10/30) columns. The histidine tags were removed by overnight digestion with tobacco etch virus protease at 4 °C. Due to the location of the tobacco etch virus cleavage site, seven residues from the histidine tag (GSSGSSG) remain at the N termini of the IL-15 and sIL-15R$\alpha^{1-168}$ proteins after histidine tag cleavage. During the gel-filtration step with 25 mM Tris-HCl buffer (pH 7.5) containing 300 mM NaCl, IL-15 eluted as a mixture of trimeric and monomeric species, and only the monomeric protein was used for subsequent experiments. For complex formation, separately refolded monomeric IL-15 and sIL-15R$\alpha^{1-168}$ were mixed at a 1.5:1 molar ratio and concentrated using an Amicon Ultra 15 filtration unit. The IL-15·sIL-15R$\alpha^{1-168}$ mixture was loaded onto a Superdex 200 HR 10/30 column equilibrated in 25 mM Tris-HCl buffer (pH 7.5) containing 150 mM NaCl and eluted at a position consistent with 1:1 complex formation, which was confirmed via analytical ultracentrifugation. Co-refolded IL-15·sIL-15R$\alpha^{1-168}$ complex behaved identically to the separately refolded and reconstituted complex during purification. The co-refolding method was utilized for large scale protein preparation due to its consistently higher yields. For large scale protein preparation, an anion exchange step (Mono Q HR 5/5) was added prior to the final gel-filtration step (which was performed using a Superdex 75 HR 16/60 column). All columns were purchased pre-packed from GE Healthcare.

*Limited Proteolysis, Crystallization, and Data Collection*—Initial crystallization trials of the IL-15·sIL-15R$\alpha^{1-168}$ complex were performed using the standard sitting drop vapor diffusion method. Despite extensive screening efforts, we were unable to obtain crystals of the complex using the full-length ectodomain of IL-15Rα. During protein synthesis and purification, we noted that the C-terminal region of sIL-15R$\alpha^{1-168}$ was extremely sensitive to proteolytic degradation, suggesting that this region of the receptor is highly flexible.

To obtain boundaries more suitable for crystallization, we performed limited proteolysis experiments on the IL-15·sIL-15R$\alpha^{1-168}$ complex. Using elastase (Nacalai Tesque), a stable fragment of the complex was identified during small scale pilot experiments, and the reaction conditions were scaled-up. The digested protein was purified by gel-filtration chromatography and analyzed using MALDI-TOF and N-terminal sequencing. The results of this analysis showed that the PT region and most of the linker region of IL-15Rα are rapidly degraded and that the stable fragment of IL-15Rα corresponds to residues 1–71, which includes the entire sushi domain and the first five residues of the linker region. The results also showed that IL-15 was not proteolytically digested. On the basis of these results a modified IL-15Rα construct (sIL-15R$\alpha^{1-71}$) was generated, synthesized, and purified in complex with IL-15 as described above for sIL-15R$\alpha^{1-168}$.

Diffraction quality crystals of the selenomethionine-labeled IL-15·sIL-15R$\alpha^{1-71}$ complex (hereafter referred to as IL-15·IL-15Rα) were grown by mixing 2 μl of IL-15·IL-15Rα (18 mg/ml in 25 mM Tris-HCl buffer (pH 7.5) containing 150 mM NaCl) with 2 μl of crystallization buffer (1.7 M sodium/potassium

phosphate, pH 6.8, 3% benzamidine-HCl) and incubating at 20 °C using hanging drop vapor diffusion. Large, single crystals measuring 0.5 mm in the longest dimension appeared within 5–7 days. Crystals were flash frozen in a final cryoprotectant solution composed of the mother liquor and 25% glycerol. Diffraction data were measured on an ADSC Quantum210 detector at Photon Factory-Advanced Ring, Beamline NW12. The data were indexed, integrated, and scaled using HKL2000 (31). The IL-15·IL-15Rα crystals belong to the tetragonal space group $P42_12$ with unit cell dimensions $a = b = 118.5$ Å, $c = 76.11$ Å. There are two IL-15·IL-15Rα complexes in the asymmetric unit, with a solvent content of ~58%.

*Structure Determination and Refinement*—The IL-15·IL-15Rα structure was solved using diffraction data collected at the selenium absorption peak wavelength (λ = 0.9793 Å) of one selenomethionine-derivatized crystal. The program SOLVE (32) was used to locate the selenium sites and to calculate the phases using the single wavelength anomalous dispersion method. The program RESOLVE (33) was used for density modification, and ARP/wARP (34) was used to generate an initial model via automatic model building. Positional and *B*-factor refinements were performed using the program CNS (35), and model building into the $2F_o - F_c$ and $F_o - F_c$ electron density maps was performed with the program O (36). The final refined atomic model contains residues 1–114 of both copies of IL-15 in the asymmetric unit, residues 3–71 in one copy of IL-15Rα, and residues 3–70 in the other copy of IL-15Rα in the asymmetric unit, 90 water molecules, and one benzamidine molecule. The remaining residues of the N-terminal histidine tag are completely disordered in both copies of IL-15Rα, whereas the last three residues of this region are ordered in both copies of IL-15 and are included in the atomic model. Additionally, residues 1–2 are disordered in both copies of IL-15Rα, and residue 71 is disordered in one copy of IL-15Rα in the asymmetric unit. The atomic coordinates and structure factors have been deposited into the Protein Data Bank under accession code 2PSM. Superimposition of the $C_\alpha$ trace of the two copies of IL-15 and the IL-15Rα shows that they are essentially identical (r.m.s.d. = 0.451 Å and 0.202 Å, respectively). Representations of the structure were created with the programs PyMOL[3] and CCP4MG (38).

*Generation of IL-15Rα- and IL-2Rβ-expressing FDC3 Cell Line*—The cDNA of full-length murine IL-15Rα and IL-2Rβ were amplified by PCR and introduced into retroviral vectors, MSCV-IRES-GFPRV and pNX-IRES-hCD4RV, respectively. The murine mast cell line, FDC-P1 (39), was purchased from ATCC, re-cloned, and renamed as FDC3. This cell line was cultured in Dulbecco's modified Eagle's medium containing 10% calf serum and conditioned media of P815 cells expressing IL3. PLAT:E packaging cell lines were transfected with IL-15Rα/MSCV-IRES-GFPRV or IL-2Rβ/pMX-IRES-hCD4RV by FuGENE according to the manufacture's instructions. After 24 h, the medium was replaced, and the retroviral supernatant was generated by culturing the cells for a further 24 h. The FDC3 cell line was infected by overnight culture in retroviral culture supernatant containing 8 mg/ml Polybrene. Infected FDC3 cell lines were purified by cell sorting for expression of the green fluorescent protein and/or the hCD4 surface markers. Sorted cells were expanded, were >90% pure, and stably expressed the retroviral markers.

*Single Cell Assay*—FDC3αβ and FDC3β cells cultured in IL-3 containing Dulbecco's modified Eagle's medium for 4 days were washed with phosphate-buffered saline three times, and cultured in IL-15-free, IL3-free Dulbecco's modified Eagle's medium with 10% calf serum for 7 h. A single cell was picked up by micropipette and transferred into a well of a Terasaki plate (Nunc, Roskilde, Denmark) containing Dulbecco's modified Eagle's medium with 10% calf serum in the presence or absence of 30 ng/ml IL-15. Cell division was checked under the microscope at 0 and 22 h of incubation.

*Thymidine Uptake Assay*—The sIL-15Rα protein used for the thymidine uptake assay was produced using a modified method of a previously published protocol (40). Briefly, the cDNA coding full-length ectodomain of murine IL-15Rα was amplified by PCR and subcloned into the pQE30 bacterial expression vector (His-sIL-15R$\alpha^{1-168}$). His-sIL-15R$\alpha^{1-168}$ was expressed in *E. coli* strain M15 cells and was purified to homogeneity by nickel affinity and gel-filtration chromatography.

Proliferation assays were set up in 96-well microtiter plates. Murine IL-15 (R&D) was diluted across the plates in the presence or absence of 1 μg/ml His-sIL-15R$\alpha^{1-168}$ protein. In the experiment using IL-15·IL-15R$\alpha^{1-168}$ complex or IL-15·IL-15R$\alpha^{1-71}$ complex, the concentrations of IL-15 were calculated based on the content of IL-15 in the complex. FDC3αβ or FDC3β cells were plated at 4000 cells in 96-well flat-bottom plate and incubated for 24 h. The plates were pulsed with [$^3$H]thymidine (0.1 μCi/well, Amersham Biosciences) for the last 6 h of culture. The cells were harvested on glass fiber filters and counted on a mutidetector direct beta counter (Matrix 96, Packard Instrument Co., Meriden, CT). Dose-response curves were generated and analyzed using GraphPad Prism.

## RESULTS AND DISCUSSION

To elucidate the structural basis for the high affinity and specificity between IL-15 and IL-15Rα, and to obtain insights into the architecture of the IL-15·IL-15R complex, we have determined the crystal structure of IL-15 in complex with IL-15Rα. Initial attempts to crystallize IL-15 in complex with the full-length ectodomain of IL-15Rα were unsuccessful. Limited proteolysis experiments performed on purified IL-15·IL-15Rα complex led to the identification of a stable IL-15Rα fragment (encompassing the sushi domain and the first five residues of the linker region) that was amenable to crystallization (see "Experimental Procedures"). The IL-15·IL-15Rα structure was solved using the single wavelength anomalous dispersion method and has been refined to 2.2-Å resolution with working and free *R* values of 22.4% and 23.6%, respectively (Table 1). As shown in Fig. 1*A*, IL-15Rα interacts with the upper edge of the IL-15 four-helix bundle.

*Structure of Receptor-bound IL-15*—The crystal structure shows that IL-15 comprises a left-handed antiparallel four-helix bundle (hA, hB, hC, and hD) with the helices arranged in an up-up-down-down topology typical of members of the short-

[3] DeLano, W. L. (2002) *PyMOL*, DeLano Scientific, San Carlos, CA.

**TABLE 1**
**Summary of crystallographic analysis**

| Data collection statistics | | | | |
|---|---|---|---|---|
| Resolution | Reflections (total/unique) | Completeness | $R_{sym}$[a] | Signal |
| Å | | % | | ⟨I/σI⟩ |
| 50.0-2.19 | 407,623/28,362 | 100 (100)[b] | 5.7 (16.3)[b] | 23.0 |

| Refinement statistics[c] | | | | | |
|---|---|---|---|---|---|
| Resolution | Reflections | $R_{cryst}/R_{free}$[d] | r.m.s.d. | | |
| | | | Bonds | Angles | *B*-factors[e] |
| Å | | % | Å | ° | Å² |
| 25.0-2.19 | 53,064 | 22.3/23.6 | 0.006 | 1.2 | 1.6 |

[a] $R_{sym} = 100 \times \Sigma_{hkl}\Sigma_i|I_i(hkl) - \langle I(hkl)\rangle|/\Sigma_{hkl}\Sigma_i I_i(hkl)$.
[b] Value in parentheses are for the highest resolution shell: 2.27-2.19 Å.
[c] The atomic model consists of 2,833 protein atoms, 90 water molecules, and 1 benzamidine molecule.
[d] $R_{cryst/free} = 100 \times \Sigma_{hkl}||F_o(hkl)| - |F_c(hkl)||/\Sigma_{hkl}|F_o(hkl)|$, where $F_o$ (>0) and $F_c$ are the observed and calculated structure factors, respectively. 5% of the reflections were used for calculation of $R_{free}$.
[e] For bonded protein atoms.

chain subfamily of helical cytokines (Fig. 1*A*) (41). As expected based on primary sequence, IL-15 contains two disulfide bridges, which the structure shows help to stabilize the conformation of the hC–hD loop in regions of the loop that engage in contacts with the receptor (Fig. 1*A*).

Despite sharing only 16% sequence identity overall, the helices that comprise the four-helix bundles of receptor bound IL-15 and IL-2 (PDB ID: 1Z92 and 2B5I) (25, 42) superimpose well, with an r.m.s.d. of 1.2 Å over 68 equivalent Cα positions (Figs. 1*B* and 2*A*). The most obvious structural differences between IL-15 and IL-2 result from differences in the length of the helices that form the core of the protein and length and conformational differences in the loop regions between the helices (hA–hB, hB–hC, and hC–hD loops) (Figs. 1*B* and 2*A*). Importantly, the hA–hB loop of IL-15 is shorter by four residues compared with that of IL-2, which prevents the formation of a helix corresponding to hA′ of IL-2 (Figs. 1*B* and 2*A*). Another important difference is observed in hB of IL-15, which adopts a more rigid and extended conformation compared with the corresponding region of IL-2 (hB and hB′), which is bent due to the presence of a proline residue (Pro-65) at the start of hB′ (Figs. 1*B* and 2*A*). IL-15 lacks a proline residue in its hB region, which permits the C-terminal extension of hB and more rigid conformation of the helix. Because hB and the hA–hB loop region account for a major portion of the ligand-receptor interface in both the IL-15·IL-15Rα and IL-2·IL-2Rα complexes, these conformational differences have an impact on the distinct modes of α receptor binding observed for these ligands (see below).

A final structural difference worth noting is the fact that hA of IL-15 is significantly shorter at its N terminus compared with hA of free or receptor-bound IL-2 from previously determined crystal structures (PDB ID: 1Z92, 2ERJ, and 2B5I) (Figs. 1*B* and 2*A*). hA of IL-2 plays a role in the assembly of the IL-2·IL-2Rα·IL-2Rβ·$\gamma_c$ complex (26) (IL-2 quaternary complex), so the significantly shorter N terminus of IL-15 relative to IL-2 has possible implications on the IL-15 mode of binding to IL-2Rβ/$\gamma_c$, which will be discussed in detail below.

*Structure of Ligand-bound IL-15Rα*—The IL-15Rα sushi domain has an elliptical structure comprised of six β-strands (βB, βC, βC′, βD, βE, and βE′) that envelope a compact hydrophobic core (Fig. 1*A*). The central β-sheet of the IL-15Rα sushi domain is formed by strands βC, βD, and βE. In typical sushi domain structures two β-strands at the N-terminal region of the domain (βA and βB) pack against the central β-sheet to form a β-sandwich arrangement (43). As noted previously in the NMR structure of unliganded human IL-15Rα sushi domain (PDB ID: 2ERS), this arrangement is not observed in the IL-15Rα sushi domain fold due to the presence of three consecutive proline residues (Pro-5, Pro-6, and Pro-7) that prevent the formation of the βA strand (Fig. 1*A*) (27). The IL-15Rα sushi domain contains two disulfide bridges: the first between Cys-4 at the N terminus of the sushi domain and Cys-46 in βD, which serves to pin the highly flexible N-terminal region to the central β-sheet of the domain, and the second between Cys-30 at the C-terminal end of the βC strand and Cys-64 in the βE′ strand, which seems to stabilize the sushi domain core (Fig. 1*A*). Comparison of our crystal structure of ligand-bound murine IL-15Rα to the NMR structure of unliganded human IL-15Rα (PDB ID: 2ERS) shows that the core of the IL-15Rα sushi domain does not undergo significant conformational changes upon ligand binding. However, the conformation of loop regions between the β-strands (outside of regions involved in ligand binding) are quite different, presumably due to inherent flexibility (data not shown).

Although IL-15Rα and IL-2Rα are structurally related in that they are composed of sushi domains, linker, and PT regions, IL-15Rα contains a single sushi domain that mediates ligand binding, whereas IL-2Rα contains two sushi domains separated by a linker region (Fig. 2*B*). The previously determined IL-2·IL-2Rα crystal structure (PDB ID: 1Z92) (42) showed that the two sushi domains of IL-2Rα engage in strand exchange and that the N-terminal sushi domain (IL-2Rα D1) participates in most of the interactions with IL-2. Superimposition of IL-2Rα D1 onto the sushi domain of IL-15Rα from the IL-15·IL-15Rα structure shows that the conformation of most of the receptor regions involved in ligand binding adopt a similar conformation (βC–βE′ region of the receptors superimpose with an r.m.s.d. of 1.73 Å) (Fig. 2*C*). In contrast, the strand-exchanged region of IL-2Rα D1 (residues 102–122), which is involved in some contacts with IL-2, adopts a significantly different conformation from the corresponding region of IL-15Rα (residues 3–20), which does not make any contacts with IL-15 (Fig. 2*C*). The effects of these structural differences on the distinct modes of IL-15·IL-15Rα and IL-2·IL-2Rα binding will be discussed below.

*IL-15·IL-15Rα Interface*—The IL-15Rα binding surface of IL-15 comprises residues from hB, hC′, and the hA–hB and hC–hD loops, whereas the IL-15 binding surface of IL-15Rα comprises residues from strands βC and βC′ and the βC′–βD and βE–βE′ loops (Fig. 1). Calculation of the surface electrostatic potential of IL-15 reveals a groove at the receptor-binding interface that is lined with acidic residues and thus possesses a striking degree of negative potential (Fig. 3*A*). Calculation of the surface electrostatic potential of IL-15Rα reveals three prominent "knobs" of positive potential located at its ligand-binding surface that are formed by Arg-25 and Arg-27 in βC, and Arg-36 in βC′ (Fig. 3*A*). In forming the IL-15·IL-15Rα com-

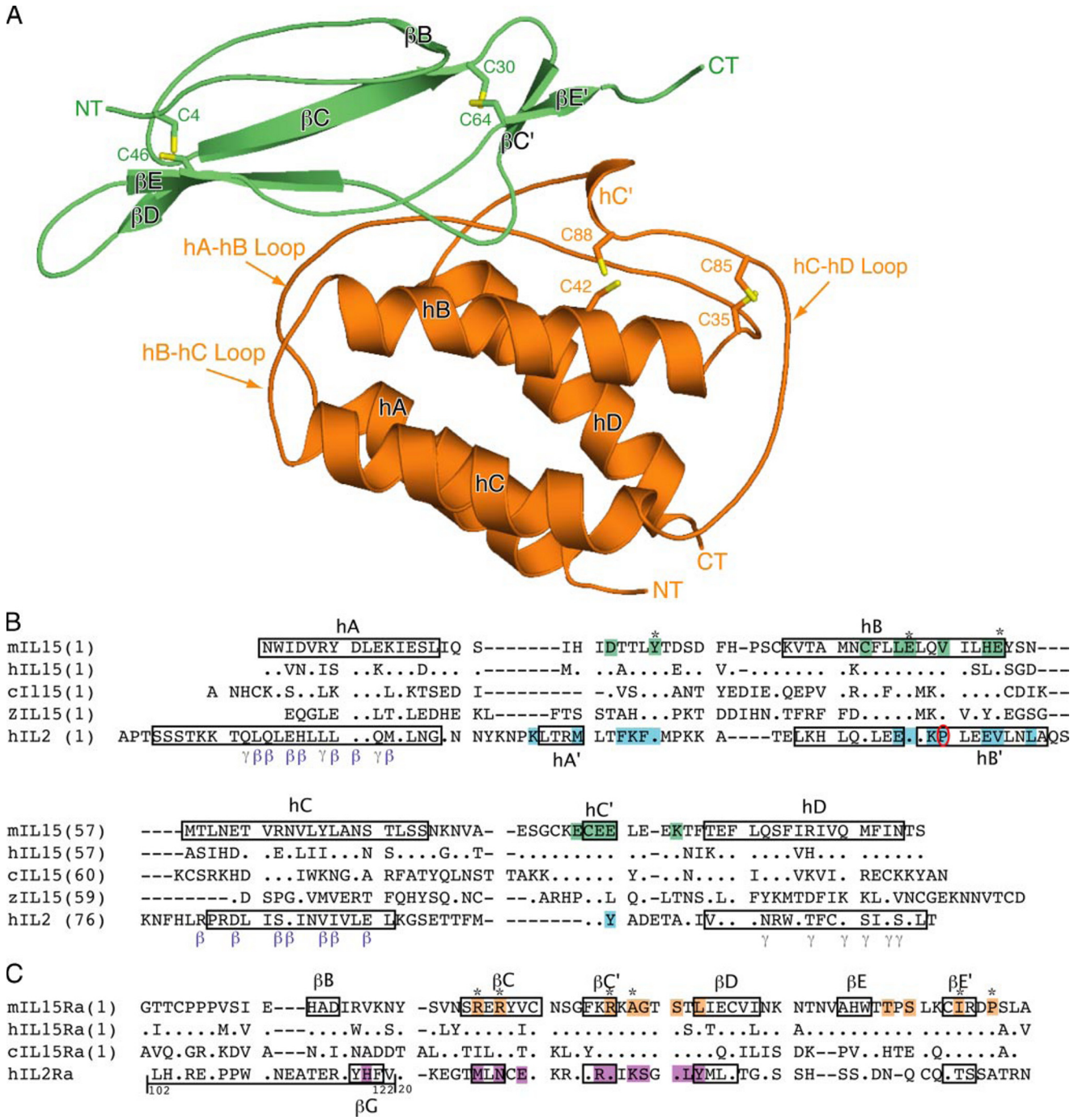


FIGURE 1. **Overall features of the IL-15·IL-15Rα complex and structure-based sequence analysis of the IL-15·IL-15Rα mode of receptor binding.** *A*, ribbon representation of the IL-15·IL-15Rα complex. IL-15 is colored *orange*, and IL-15Rα is colored *green*. Secondary structure assignments were performed using PROCHECK (37). The β-strands of IL-15Rα and helices of IL-15 are labeled according to the conventional nomenclature for these proteins. The side chains of cysteine residues that participate in intramolecular disulfide bridge formation in IL-15 and IL-15Rα are shown as *sticks*, and their sulfur atoms are colored *yellow*. The N and C termini of are labeled *NT* and *CT*, respectively. All figures present the copy of the IL-15·IL-15Rα complex from the asymmetric unit that had stronger electron density. All figures were prepared using the program PyMOL unless noted otherwise. *B* and *C*, structure-based sequence alignment of selected interleukins (*B*) and interleukin receptor alpha sushi domains (*C*). Predicted signal sequences have been omitted from the alignment. Residue numbers are in *bold font* to the *left* of the sequence alignment. All proteins are numbered starting from the first residue after predicted signal peptide cleavage. A *dash* represents a gap introduced to optimize the alignment. The locations of the secondary structural elements are indicated by *black boxes*. The proline residue in the IL-2 that contributes to the bent conformation of the hB–hB′ region is *circled* in *red*. IL-15 residues that interact with IL-15Rα are *shaded green*, IL-15Rα residues that interact with IL-15 are *shaded orange*, IL-2 residues that interact with IL-2Rα are *shaded cyan*, and IL-2Rα residues that interact with IL-2 are *shaded purple*. IL-15 and IL-15Rα residues that play a particularly important role in determining the unique mode IL-15·IL-15Rα specificity are marked with an *asterisk*. IL-2 residues that interact with IL-2Rβ or IL-2Rγ$_c$ in the IL-2 quaternary complex (25, 26) (PDB IDs: 2B5I and 2ERJ) are indicated with β or γ, respectively, below the sequence alignment. The sequences of *D. rerio* IL-15 (zIL-15), *G. gallus* IL-15 (cIL-15), and *G. gallus* IL-15Rα (cIL-15Rα) are shown to highlight the evolutionary conservation of the IL-15·IL-15Rα mode of binding, which is unique among cytokine·cytokine receptor complexes.

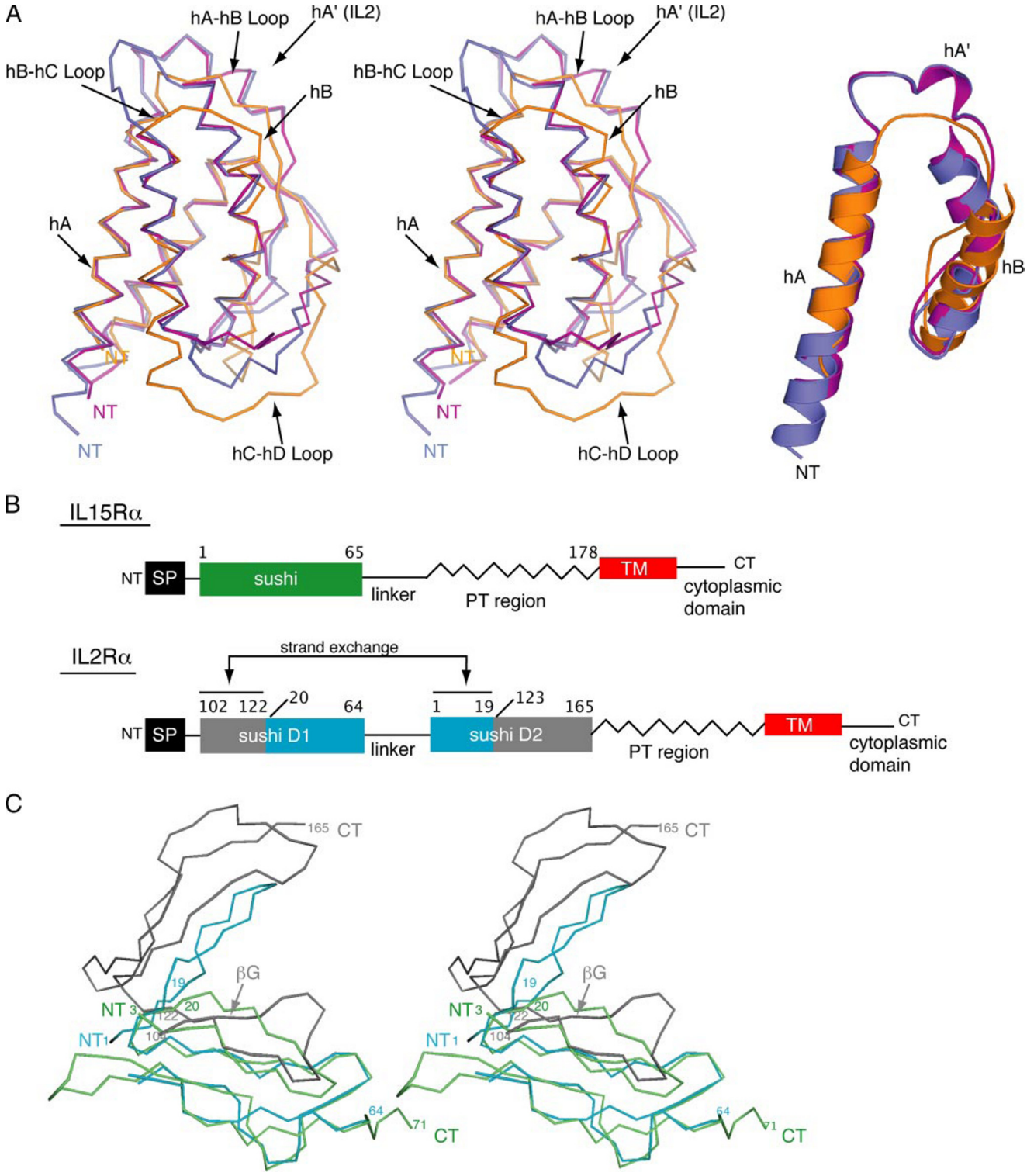


FIGURE 2. **Comparison of the structural features of IL-15, IL-2, and their alpha receptors.** *A*, comparison of the conformations of receptor-bound IL-15 and receptor-bound IL-2. The Cα traces of IL-2 from the IL-2·IL-2Rα structure (PDB ID: 1Z92) and IL-2 from the IL-2 quaternary complex structure (PDB ID: 2B5I) were superimposed onto the Cα trace of receptor bound IL-15 (r.m.s.d. = 1.3 Å and 1.2 Å, respectively). The superimposed structures are shown in *stereoview*. IL-15 is colored *orange*, IL-2 from the IL-2·IL-2Rα complex is colored *purple*, and IL-2 from the IL-2 quaternary complex is colored *blue*. N and C termini of IL-15 and IL-2 are labeled *NT* and *CT*, respectively. Structural differences observed between IL-15 and IL-2 with implications on receptor binding are indicated with *arrows*. These differences are highlighted by the *right panel*, in which the only the regions encompassing the N terminus of hA to the C terminus of hB of receptor-bound IL-15 and IL-2 are shown as ribbon representations for clarity. *B*, schematic diagram of the domain organization of IL-15Rα and IL-2Rα. Signal peptides and transmembrane domains are labeled *SP* and *TM*, respectively. N and C termini are labeled *NT* and *CT*, respectively. Selected residue numbers are indicated above the diagram. In IL-2Rα sushi domains 1 and 2 engage in a strand exchange event in which residues 1–19 are swapped with residues 102–122, which is indicated with a *double-headed arrow* and color coding. Due to the strand exchange, residues 1–19 of IL-2Rα are a part of sushi domain 2 and residues 102–122 are a part of sushi domain 1. *C*, comparison of the conformations of ligand-bound IL-15Rα and ligand-bound IL-2Rα. The Cα trace of ligand-bound IL-2Rα D1 (PDB ID: 1Z92) was superimposed onto the Cα trace of receptor bound IL-15Rα (r.m.s.d. = 1.3 Å). IL-15Rα is colored *green*, residues 1–64 of IL-2Rα are colored *cyan*, and residues 104–165 are colored *gray*. Note the presence of only one sushi domain in IL-15Rα *versus* two strand-swapped sushi domains in IL-2Rα.

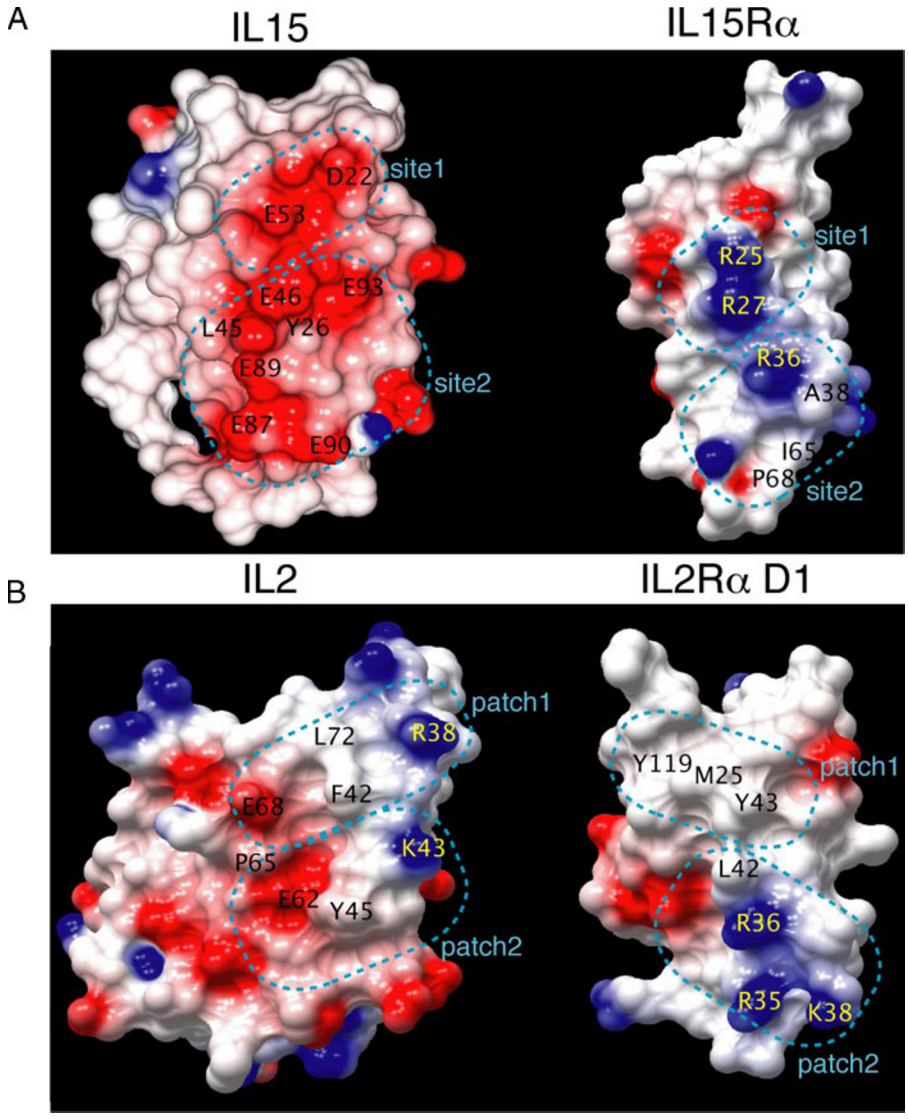


FIGURE 3. **Comparison of surface electrostatic charge at the IL-15·IL-15Rα and IL-2·IL-2Rα interfaces.** *A*, IL-15·IL-15Rα and *B*, IL-2·IL-2Rα complexes are shown as molecular surface representations in an *open book view*. Selected residues are labeled. Electrostatic potentials are mapped onto the molecular surfaces, with negative potential colored *red* and positive potential colored *blue*. Sites 1 and 2 of the IL-15·IL-15Rα complex and patches 1 and 2 of IL-2·IL-2Rα complex are indicated with a *dashed cyan line* and labeled. Note the presence of a negatively charged groove on IL-15 into which the three knobs of positive potential (Arg-25, Arg-27, and Arg-36) insert. The electrostatic potentials were calculated, and the figure was prepared using the program CCP4mg (38).

plex, the IL-15Rα knobs insert into the groove of IL-15 to form an interlocking interface with good charge and shape complementarity ($S_c$ = 0.73) and high specificity (14 direct hydrogen bonds). 14 residues from IL-15 and 15 residues from IL-15Rα bury a total surface area of 1240 Å$^2$ at the IL-15·IL-15Rα interface.

Analysis of the interactions at the IL-15·IL-15Rα interface reveal two adjacent concentrated clusters of primarily hydrogen bond-mediated interactions (termed *sites 1* and *2*, Fig. 4, *A* and *B*), which likely account for most of the binding energy of the complex. At the center of site 1, Arg-27 in βC of IL-15Rα forms salt bridges with Glu-53 at the C-terminal tip of hB and Asp-22 in the hA–hB loop of IL-15 (Fig. 4*A*). As shown in Fig. 4*A*, these central salt bridges are surrounded by additional contacts between residues in hB of IL-15 and the βC′–βD and βE-βE′ loops of IL-15Rα. The set of interactions observed at site 1 is unique to the IL-15·IL-15Rα complex and constitutes a major determinant of the unique mode of IL-15·IL-15Rα binding (see below).

Arg-36 of IL-15Rα is at the center of the network of hydrogen bonds that take place at site 2 of the IL-15·IL-15Rα interface. Here, Arg-36 of IL-15Rα forms salt bridges with Glu-46 in the middle of hB and Glu-93 in the hC–hD loop of IL-15 (Fig. 4*B*). Adjacent to this set of interactions, Tyr-26 and Glu-46 of IL-15 engage in hydrogen bonds with the backbone oxygen of Arg-36 and the backbone nitrogen of Gly-39, respectively, in IL-15Rα (Fig. 4*B*). Although most of the contacts at the IL-15·IL-15Rα interface are hydrogen bond-mediated, there are a few important hydrophobic interactions that take place at site 2. The first of these hydrophobic contacts is mediated by the methyl group of Ala-38 at the tip of the βC′–βD loop of IL-15Rα, which inserts into a prominent hydrophobic pocket formed by Tyr-26, Leu-45, and Val-49 and a partially solvent-exposed disulfide bridge between Cys-42 and Cys-88 in IL-15 (Fig. 4*B*). This interaction strengthens the site 2 interface directly via binding and contributes to the exclusion of bulk solvent by capping one end of the IL-15·IL-15Rα interface. Adjacent to this interaction, Ile-65 and Pro-68 in the βE′ and linker regions, respectively, of IL-15Rα, pack against a hydrophobic patch formed by the aliphatic portion of the side chains of Glu-87, Glu-89, and Glu-90 in hC′ and the hC–hD loop of IL-15 (Fig. 4*B*). This set of hydrophobic interactions at site 2 is unique to the IL-15·IL-15Rα interface and, in addition to site 1 interactions, play a role in determining IL-15·IL-15Rα specificity (see below).

The residues involved in the key interactions identified in the murine IL-15·IL-15Rα crystal structure are in good agreement with published mutagenesis studies (15, 28). Scatchard analysis using human proteins shows that mutation of IL-15Rα Arg-36 to threonine results in an 80-fold decrease in affinity for IL-15 (28), and mutation of IL-15 Glu-46 to lysine results in a complete loss in affinity for IL-15Rα (15), underscoring the importance of the site 2 interactions to general binding affinity. Furthermore, sequence alignment shows that all of the key residues involved in murine IL-15 and IL-15Rα complex formation,

including Arg-27, Arg-36, and Ala-38 of IL-15Rα and Tyr-26, Glu-46, and Glu-53 of IL-15, are fully conserved in all vertebrate IL-15 and IL-15Rα orthologs for which sequence information is available (Fig. 1, *B* and *C*). This suggests that the IL-15·IL-15Rα mode of binding has been conserved throughout evolution, and thus, our structure provides the molecular basis for the high affinity and specificity of the IL-15·IL-15Rα complex for all vertebrates.

This hypothesis has been reinforced by the recently determined human IL-15·IL-15Rα crystal structure, which was published by Chirifu *et al.* (44) during the preparation of this report (PDB ID: 2Z3Q and 2Z3R). The structures of the human and mouse orthologs of IL-15 and IL-15Rα are similar (supplemental Fig. S1, *A* and *B*), and as expected the interactions at sites 1 and 2 are conserved (supplemental Fig. S1, *C* and *D*). One unexpected structural difference between the human and mouse IL-15 proteins is that, although hB of both orthologs adopts the same extended conformation (which permits Glu-53 at the tip of hB to salt bridge with Arg-27 of IL-15Rα), the orientation of hB (IL-15Rα binding site) relative to helices A, C, and D (IL2Rβ/$\gamma_c$ binding site), is slightly different between the two structures (supplemental Fig. S1*A*). This appears to be due to sequence divergence in the hB–hC loop of the ligands, in particular Tyr-54 (which is Ser-54 in human IL-15) (Fig. 1*B*), which would severely clash with residues in hB, hC, and the hA–hB loop if murine IL-15 adopted the same structure as human IL-15 in this region (supplemental Fig. S2).

*IL-15·IL-15Rα Mode of Binding Is Distinct from That of IL-2·IL-2Rα and Other Cytokine·Cytokine Receptor Complexes*—In marked contrast to the IL-15·IL-15Rα interface, which is dominated by salt bridges/hydrogen bonds, the IL-2·IL-2Rα interface (PDB ID: 1Z92) is dominated by hydrophobic interactions at its center, which are surrounded

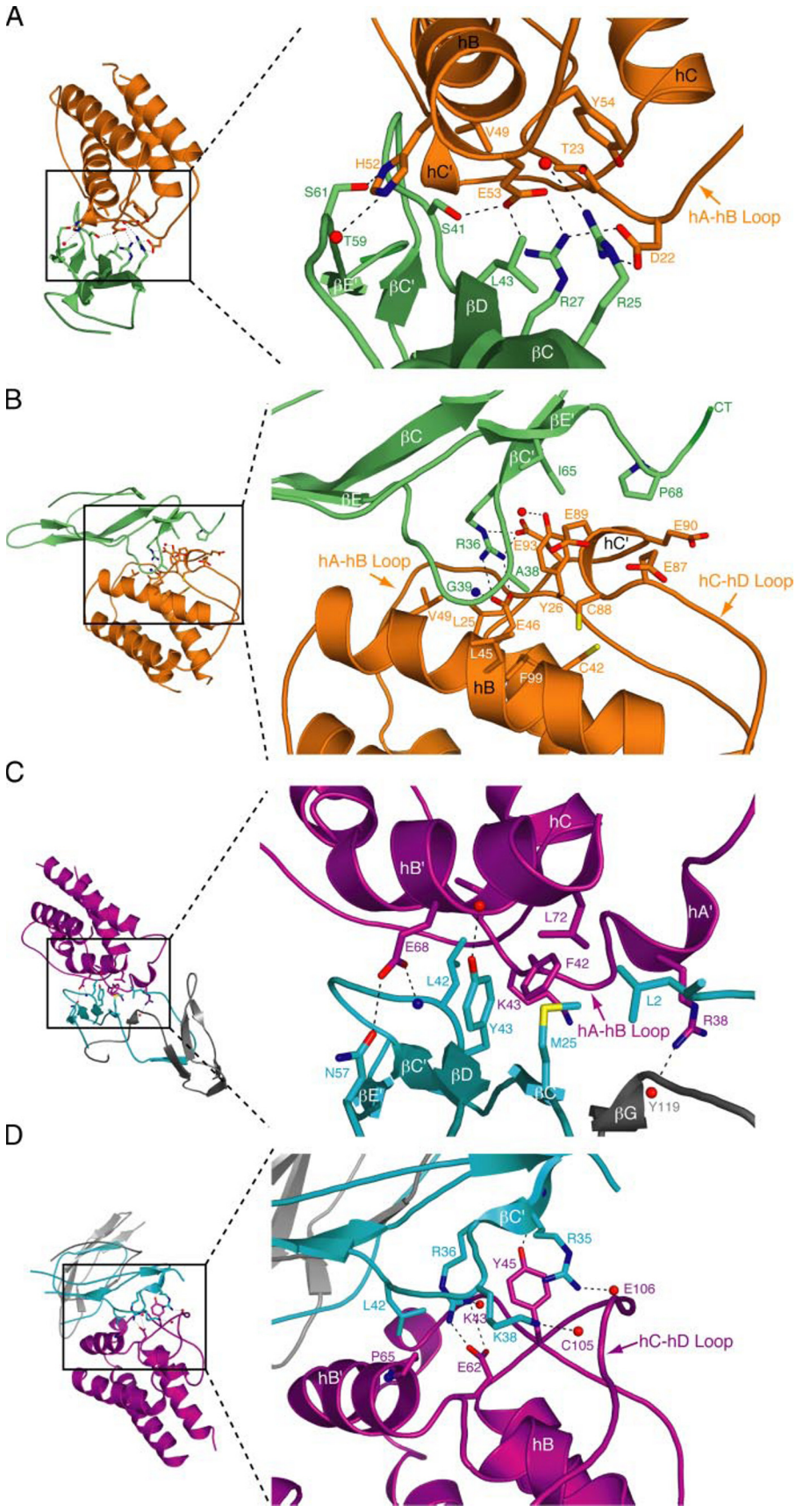

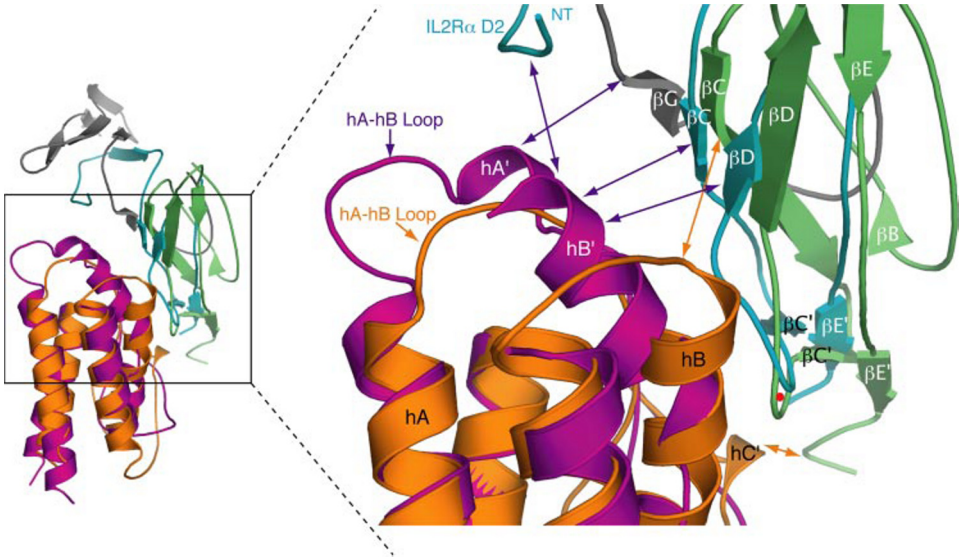


FIGURE 5. **Superimposition of IL-15·IL-15Rα and IL-2·IL-2Rα structures highlights distinct modes of binding.** The Cα trace of IL-2 from the IL-2·IL-2Rα complex (PDB ID: 1Z92) was superimposed onto IL-15 from the IL-15·IL-15Rα complex as in Fig. 2. Ligand and receptor from both complexes are shown as *ribbon representations* and are *colored* as in Fig. 2. Regions of the complexes that engage in unique contacts are indicated with *arrows*. Note that IL-15 and IL-2 superimpose well with one another, but that there is a slight rotation of the receptors relative to one another, which allows the formation of specific contacts in the IL-15·IL-15Rα and IL-2·IL-2Rα complexes. Also note that distinct features of IL-2, including a longer hA–hB loop (and presence of hA′) and the kink in hB (resulting in hB′) enable unique contacts with the bottom edge of IL-2Rα D2, the βG strand from the strand-swapped region of D1, and the βD strand (refer to Fig. 4*C*). The extended hB of IL-15 and differences in sequence allow for unique contacts with the βC strand IL-15Rα (refer to Fig. 4*A*). The pivot point of the rotation is marked with a *red circle* and corresponds to residue Ala-38 of IL-15 and Lys-38 of IL-2, which are located in site 2/patch 2 of the IL-15·IL-15Rα and IL-2·IL-2Rα interfaces (refer to Fig. 4, *B* and *D*).

by polar interactions (42). As predicted by Lorenzen *et al.* (27) based on molecular modeling, calculation of surface electrostatic potential of IL-15 and IL-15Rα from our crystal structure shows that the IL-15·IL-15Rα interface contains more charged residues and exhibits a higher degree of charge and shape complementarity compared with the IL-2·IL-2Rα interface (compare Fig. 3, *A* and *B*). Rickert *et al.* identified two critical interaction sites at the IL-2·IL-2Rα interface: one centered around Phe-42 in the hA–hB loop of IL-2 (*patch 1*, Fig. 4*C*) and the second centered around Tyr-45 in the hA–hB loop of IL-2 (*patch 2*, Fig. 4*D*) (42). To compare their modes of binding, we superimposed IL-2 from the IL-2·IL-2Rα structure (PDB ID: 1Z92) onto IL-15 from our IL-15·IL-15Rα structure. Interestingly, the superimposition shows that, despite the considerably different nature of their interactions, patch 1 and patch 2 of the IL-2·IL-2Rα interface overlap well with site 1 and site 2 of the IL-15·IL-15Rα interface (Fig. 4, compare *A* with *C*, and *B* with *D*).

At patch 1 of the IL-2·IL-2Rα interface, hA′ and hB′ of IL-2 adopt a significantly different conformation than the corresponding regions at site 1 of IL-15 (Fig. 4, compare *C* and *A*). In the IL-2·IL-2Rα structure, hA′ and hB′ lie roughly parallel to one another and form an interface with the unique strand-swapped regions of sushi domain 1 (particularly βG) and sushi domain 2 (particularly the N terminus) of IL-2Rα (Fig. 4*C*). Although these interactions account for only a small portion of the IL-2·IL-2Rα interface and are slightly different in each of the three IL-2·IL-2Rα-containing crystal structures due to crystal packing (PDB IDs: 2B5I, 1Z92, and 2ERJ), they are significant in terms of binding mechanism, because they result in a slight rotation of IL-2Rα relative to IL-15Rα, which has only one sushi domain and thus cannot participate in equivalent interactions (Fig. 5). Importantly, Leu-42 and Tyr-43 of IL-2Rα βD are brought into the vicinity of Phe-42 due to the relative rotation of IL-2Rα, where they engage in a hydrophobic interaction that acts as the primary energetic determinant in the IL-2 binding epitope (Figs. 4*C* and 5) (42). The overall result of this relative rotation is that residues with different physicochemical properties and from different regions of the receptor and ligand form the functional epitopes at the IL-2·IL-2Rα and IL-15·IL-15Rα interfaces (Fig. 4, compare *C* and *A*).

Compared with site 1/patch 1, the superimposition shows that the nature of the interactions at site 2/patch 2 of the IL-15·IL-15Rα and IL-2·IL-2Rα interfaces are better conserved (Fig. 4, compare *D* and *B*). Patch 2 at the IL-2·IL-2Rα interface is centered around Tyr-45 in the hA–hB loop of IL-2, which packs against the aliphatic part of Arg-35 and Arg-36 from the βC′ strand of IL-2Rα and engages in a hydrogen bond with the backbone nitrogen of Arg-35 (Fig. 4*D*). Surrounding this central hydrophobic cluster are several polar interactions, including a salt bridge between Arg-36 of IL-2Rα and Glu-62 of IL-2 (Fig. 4*D*). Interestingly, this salt bridge corresponds to the salt bridge between Arg-36 of IL-15Rα and Glu-46 of IL-15 (Fig. 4, compare *D* and *B*). Tyr-45 of IL-2 is also conserved in IL-15 (Tyr-26, Fig. 1*B*), however, Tyr-26 of IL-15 engages in a distinct set of interactions with the receptor in the IL-15·IL-15Rα structure (Fig. 4*B*). Superimposition shows that site 2/patch 2 serves as the pivot point of the relative rotation observed at the IL-2·IL-2Rα and IL-15·IL-15Rα interfaces (Fig. 5), which is not surprising considering the conservation of key interactions at this region mentioned above.

FIGURE 4. **Comparison of interactions at the IL-15·IL-15Rα and IL-2·IL-2Rα interfaces.** *A–D*, analysis of interactions at site 1 (*A*) and site 2 (*B*) of the IL-15·IL-15Rα interface and patch 1 (*C*) and patch 2 (*D*) of the IL-2·IL-2Rα interface. The IL-15·IL-15Rα and IL-2·IL-2Rα complexes are shown as *ribbon representations*. IL-15·IL-15Rα, IL-2, and IL-2Rα are *colored* as in Fig. 2. Selected residues are labeled and side chains are rendered as *sticks*. Hydrogen bonds are shown as *dashed black lines*. Carbons, nitrogens, oxygens, and sulfur atoms are colored *orange*, *blue*, *red*, and *yellow*, respectively. For *each panel*, the magnified regions of interest are shown on the *right side*, and to allow for perspective, an overview of the entire structure is presented in the same orientation in the *left panel* with the region of interest *boxed*. To allow for direct comparison of the IL-15·IL-15Rα and IL-2·IL-2Rα interfaces *panels A* and *C* are shown in the same orientation, and *panels B* and *D* are shown in the same orientation.

IL-15Rα and IL-2Rα have similar domain composition, share limited sequence homology, and together are unique among cytokine receptors in that sushi domains mediate interactions with their specific four-helix bundle cytokines. However, despite these similarities, comparison of the structures shows that the IL-15·IL-15Rα and IL-2·IL-2Rα modes of binding have diverged during evolution. The nature of the interactions at the IL-2·IL-2Rα interface resembles those of cytokine·cytokine receptor complexes such as growth hormone·growth hormone receptor (PDB ID: 3HHR) (45) and GCSF·GCSFR (PDB ID: 1PGR) (46) complexes, which are dominated by hydrophobic contacts, whereas the nature of interactions at the IL-15·IL-15Rα interface resembles the hydrogen bond-dominated "avocado clusters" observed at the IL4·IL4Rα interface (PDB ID: 1IAR) (47), or the mosaic, interlocking interface of the p35·p40 complex of IL12 (PDB ID: 1F45) (48). A functional consequence of this divergence between IL-15·IL-15Rα and IL-2·IL-2Rα is that it results in complexes with different affinities, which may account for the inherently different signaling properties and biological activities of IL-15 and IL-2 by modulating the strength and duration of signaling by the $\beta\gamma_c$ complex. Indeed, it has recently been demonstrated that IL-15 is unique among cytokines due to its persistent *in vivo* activity and ability to mediate prolonged signaling in $CD8^+$ T cells (13). Consistent with this observation, IL-15 is predominantly detected in complex with IL-15Rα at the plasma membrane (effectively increasing its local concentration), and upon endocytosis these IL-15·IL-15Rα complexes are stable and can be effectively recycled back to the cell surface ("intercellular reservoir effect" (13, 22)). It has been suggested that both of these unique properties of IL-15 may be mediated by the high affinity and enhanced stability of the IL-15·IL-15Rα complex (13, 22, 29, 49).

The binding kinetics of the IL-15·IL-15Rα and IL-2·IL-2Rα interactions have previously been analyzed using surface plasmon resonance (16, 50). These studies have shown that, although the $k_{on}$ of the IL-15·IL-15Rα and IL-2·IL-2Rα interactions are comparable, the $k_{off}$ of the IL-15·IL-15Rα interaction is more that 4 orders of magnitude slower compared with the IL-2·IL-2Rα interaction. Because $k_{off}$ is determined by the strength of short range interactions, it is likely that the additional salt bridges observed in the IL-15·IL-15Rα complex at sites 1 and 2 and the excellent shape complementarity at the IL-15·IL-15Rα interface are the main determinants of its slower $k_{off}$, and thus, higher affinity. Importantly, the IL-15·IL-15Rα crystal structure will provide an excellent molecular framework for the determination of the precise contributions of the individual interactions to the thermodynamics and kinetics of the IL-15·IL-15Rα interaction in future studies.

*IL-15·IL-15Rα·IL-2Rβ·$\gamma_c$ Quaternary Complex Model and Biochemical Evidence for cis Presentation of IL-15*—Previously published mutagenesis studies have suggested that IL-15 and IL-2 share similar interaction surfaces for IL-15Rβ and $\gamma_c$ (51). To gain insights into the architecture of IL-15 and IL-15R subunits during receptor activation, we created a model of the IL-15·IL-15Rα·IL-2Rβ·$\gamma_c$ complex by superimposing IL-15 and IL-15Rα from the IL-15·IL-15Rα crystal structure onto IL-2 and IL-2Rα from the IL-2 quaternary complex structure (PDB ID: 2B5I) (Fig. 6*A*). The IL-15·IL-15Rα·IL-2Rβ·$\gamma_c$ complex model shows that the interaction surface of IL-15 and IL-2 for their respective α receptors is also shared, and comparison of the topology of IL-15·IL-15Rα and IL-2·IL-2Rα structures shows that, with respect to the polarity of their N and C termini, IL-15 and IL-15Rα are oriented similarly to IL-2 and IL-2Rα at the ligand-receptor interface. Together, these findings are somewhat surprising considering the ability of IL-15Rα to mediate *trans* IL-15 presentation and suggest that IL-15Rα should be capable of presenting IL-15 in *cis* to IL-2Rβ/$\gamma_c$ in a manner reminiscent of the IL-2·IL-2Rα·IL-2Rβ·$\gamma_c$ complex. With respect to previously published models of the IL-15·IL-15Rα complex, the topology of the IL-15·IL-15Rα complex revealed by our crystal structure most resemble the models proposed by Lorenzen *et al.* (27) and "docking solution 2" described by Quemener *et al.* (28).

To test the ability of IL-15Rα to present IL-15 in *cis* to IL-2Rβ/$\gamma_c$ on the surface of the same cell, we utilized the mouse mast cell line FDC3, which normally express the $\gamma_c$ subunit of IL-15R, but not IL-15Rα or IL-2Rβ. FDC3 cells were infected with retroviruses expressing full-length murine IL-2Rβ only (FDC3β) or murine IL-15Rα and IL-2Rβ (FDC3αβ), and we employed the use of a single cell proliferation assay in which the ability of a single cell to proliferate in response to IL-15 is tested, thereby eliminating the possibility of *trans* presentation. As shown in Fig. 6*B*, a single FDC3αβ cell was consistently able to proliferate in the presence of 30 ng/ml IL-15, whereas FDC3β did not, clearly demonstrating that *cis* presentation can indeed occur.

We next decided to analyze the efficiency of *cis versus trans* IL-15 presentation by comparing the effect that soluble IL-15Rα and soluble IL-15·IL-15Rα complex have on the ability of IL-15 to induce proliferation in FDC3β *versus* FDC3αβ cells. As shown in Fig. 6 (*C* and *D*), FDC3β cells could proliferate only in the presence of high concentration ($EC_{50} \approx 100$ ng/ml) of murine IL-15 alone, whereas the proliferative capacity of IL-15 was markedly enhanced in the presence of His-sIL-15Rα$^{1-168}$ or IL-15·sIL-15Rα$^{1-168}$ complex ($EC_{50} \approx 3$ ng/ml). Importantly, the IL-15·sIL-15Rα$^{1-71}$ complex behaved nearly identically to the IL-15·sIL-15Rα$^{1-168}$ complex with respect to the enhancement of IL-15 activity on FDC3β cells (Fig. 6*D*), demonstrating that the IL-15Rα fragment crystallized in this study (residues 1–71) is responsible for the enhanced biological activity of IL-15. Interestingly, in contrast to the enhancing activity of soluble IL-15Rα on FDC3β cells, the proliferative capacity of IL-15 on FDC3αβ cells was decreased in the presence of His-sIL-15Rα$^{1-168}$ ($EC_{50} \approx 3$ ng/ml) compared with IL-15 alone ($EC_{50} \approx 0.05$ ng/ml).

Cumulatively, the above results indicate that IL-15 is most active when it is presented in *cis* by membrane-bound IL-15Rα to IL-2Rβ/$\gamma_c$ on the surface of the same FDC3αβ cell. In this context, soluble IL-15Rα inhibits the activity of IL-15 presumably by competing with membrane-bound IL-15Rα for IL-15. When *trans* presentation is forced (on FDC3β cells), soluble IL-15Rα enhances the activity of IL-15 relative to IL-15 alone, but IL-15 signaling in this context is never as effective as *cis* presentation on FDC3αβ cells. The molecular basis by which soluble IL-15Rα enhances the activity of IL-15 on FDC3β cells

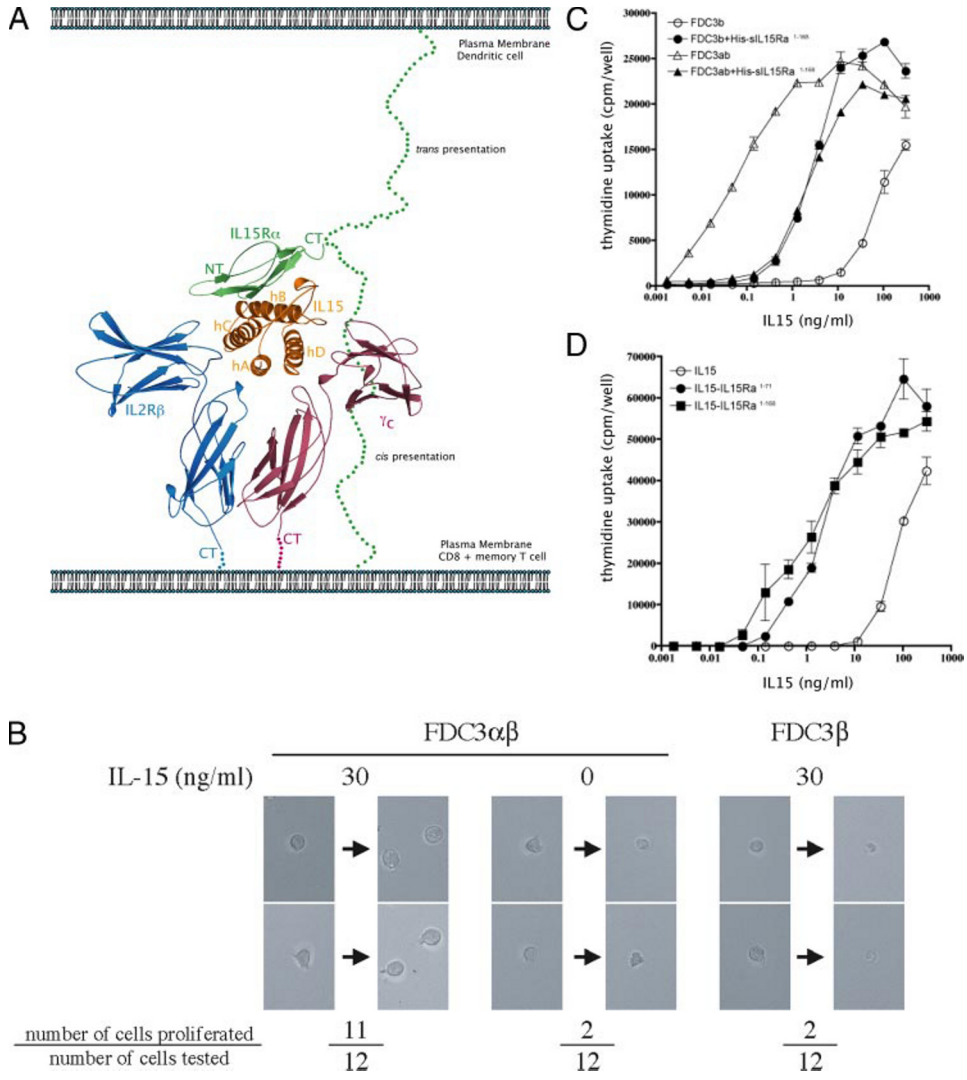


FIGURE 6. **IL-15 quaternary complex model and biochemical evidence of *cis* IL-15 presentation.** *A*, IL-15 quaternary complex model. IL-2 from the IL-2 quaternary complex (PDB ID: 2B5I) was superimposed onto IL-15 from the IL-15·IL-15Rα complex. IL-15 is colored *orange*, IL-15Rα is colored *green*, IL-2Rβ is colored *blue*, and $\gamma_c$ is colored *rose*. For clarity, IL-2 and IL-2Rα are not shown. Note the location of the C terminus of IL-15Rα, which lies in a plane that is nearly parallel to the plasma membrane. The linker region and PT region of IL-15Rα, which are not visualized in the IL-15·IL-15Rα structure are modeled as *green dots*. We propose that flexibility in the linker region and PT region of IL-15Rα allows IL-15Rα to present IL-15 in *cis* or *trans* and that the architecture of IL-15 and IL-15R components at the quaternary complex interface are the same for both modes of IL-15 presentation. *B*, *cis* presentation of IL-15 by IL-15Rα on the surface of a single FDC3αβ cell. The single cell assay was performed in a Terasaki plate. FDC3αβ and FDC3β cells were starved for cytokine for 7 h, transferred into a Terasaki plate (one cell per well), and cultured in the media containing 0 or 30 ng/ml IL-15 for 22 h. Typical *images* taken just after starting the culture and 22 h after the culture of the same cell are shown. Only FDC3αβ cultured in the presence of IL-15 can proliferate, indicating that IL-15Rα expressed on FDC3αβ present IL-15 to IL-2Rβ/$\gamma_c$ on the same cell. *C*, effect of soluble IL-15Rα protein on the thymidine uptake of FDC3 expressing IL-2Rβ and/or IL-15Rα. FDC3β required many IL-15 to uptake thymidine (*open circle*). In the presence of soluble IL-15Rα protein (His-sIL-15Ra$^{1-168}$), the required amount of IL-15 was reduced (*closed circle*). In contrast to FDC3β, FDC3αβ required very low amount of IL-15 to uptake thymidine (*open triangle*). In the presence of His-sIL-15Rα$^{1-168}$ protein, the required amount of IL-15 was increased (*closed triangle*). *D*, thymidine uptake of FDC3β stimulated with IL-15 (*open circle*), complex of IL-15·IL-15Rα$^{1-71}$ (*closed circle*), and complex of IL-15·IL-15Rα$^{1-168}$ (*closed square*). The complex of IL-15·IL-15Rα$^{1-71}$ was crystallized in this study. The residues 1–71 of mature IL-15Rα contain full-length sushi-domain and first five residues of linker region. The complex of IL-15·IL-15Rα$^{1-71}$ and IL-15·IL-15Rα$^{1-168}$ shows similar proliferation curve, indicating that IL-15Rα$^{1-71}$ is mainly responsible for the enhancement of FDC3β proliferation induced by IL-15.

is unclear, but has been suggested to be due to a conformational change induced in IL-15 upon receptor binding that enhances signaling through IL-2Rβ/$\gamma_c$ (29).

In the context of the above data, how then is IL-15Rα able to engage in both *cis* and *trans* presentation of IL-15 to IL-2Rβ/$\gamma_c$? The C terminus of the IL-15Rα ectodomain of consists of a 32-residue linker region and 74-residue PT region that exhibits a high degree of flexibility and thus were not included in the IL-15Rα protein used for crystallization (see "Experimental Procedures"). Analysis of the IL-15 quaternary complex model shows that the C-terminal-most ordered residue of IL-15Rα (Arg-71) lies in a plane that is nearly parallel with the cell surface (Fig. 6*A*). In the context of our structural and biochemical data, we propose a model in which the highly flexible nature of the linker and/or PT regions of IL-15Rα allow for the presentation of IL-15 in *cis* or *trans*, and that the orientation of IL-15 and its receptor components at the quaternary complex interface are the same whether IL-15 is presented in *cis* or *trans* (Fig. 6*A*).

According to this model, during *cis* presentation, the PT region of IL-15Rα serves to extend the IL-15-binding sushi domain far enough from the plasma membrane so that IL-15 can be productively presented to IL-2Rβ/$\gamma_c$. During *trans* presentation, the IL-15Rα sushi domain must also be extended from the plasma membrane to present IL-15 to IL-2Rβ/$\gamma_c$ of the recipient cell. However, because the orientation of the IL-15 binding surface of the *trans*-acting IL-15Rα would be opposite to that of a *cis*-acting IL-15Rα molecule, a highly flexible region of the IL-15Rα (most likely the linker region or N-terminal portion of the PT region) must adopt a conformation that allows the proper presentation of IL-15 to the IL-2Rβ/$\gamma_c$ in *trans*. The precise role of the linker region and PT region in *cis* and *trans* presentation is currently unresolved and is the subject of ongoing biochemical and structural studies.

Interestingly, alternatively spliced isoforms of IL-15 lacking the linker region (exon 3), the linker region, and part of the PT region (exons 3 and 4) or the linker region and the entire PT region (exons 3–5) have been discovered (23, 52). It will be particularly interesting to test the biological activities of each of these isoforms in context of their ability to participate in *trans versus cis* presentation. More recently, it has been demonstrated that alternative splicing of IL-15Rα gener-

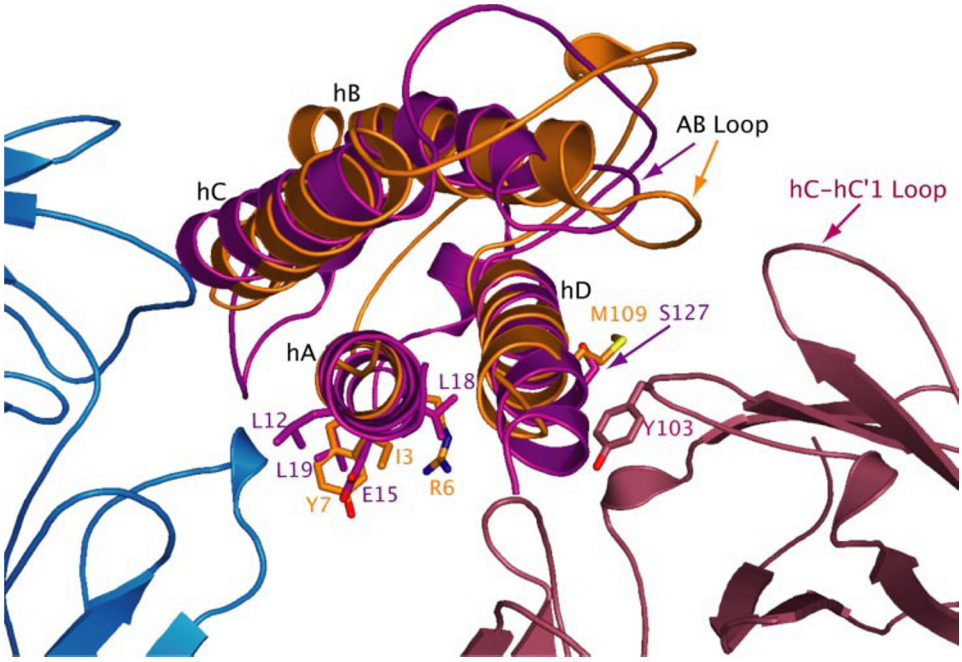


FIGURE 7. **Comparison of IL-15 quaternary complex model and IL-2 quaternary complex.** The superimposed structures are shown as *ribbon representations* and are *colored* as in Fig. 6*A*. Note that the distinct conformation of the hA–hB loop of IL-15 places this region of the ligand into the vicinity of the hC–hC′1 loop of $\gamma_c$ where unique interactions can potentially take place. Also note the position and length of hA of IL-15 and IL-2 quaternary complex interface. IL-2 residues Leu-12, Glu-15, Leu-18, and Leu-19 from the N-terminal portion of hA participate in interactions at a three-way junction between IL-2·IL-2R$\beta$ and $\gamma_c$ that is suggested to mediate cooperative binding. Due to the shorter hA of IL-15, it has no homologous residue to Leu-12 of IL-2. Furthermore, IL-2 residues Glu-15, Leu-18, and Leu-19 have diverged to Ile-3, Arg-6, and Tyr-7 in IL-15 making it unlikely that a homologous set of interactions takes place at the IL-15·IL-2R$\beta$/$\gamma_c$ junction.

ates soluble IL-15R sushi domain that forms a complex with IL-15 and is capable of signaling through the IL-2R$\beta$/$\gamma_c$ (23). Bulanova *et al.* (23) suggest that, in addition to the membrane-bound IL-15·IL-15R$\alpha$ complex, these alternatively spliced sushi domains may also play an important role in IL-15 *trans* presentation *in vivo*, and by extension of our model, we propose that these complexes exhibit the same architecture as presented in Fig. 6*A*.

*Insights into the IL-2Rβ and $\gamma_c$ Receptor Binding Sites of IL-15*—Consistent with the hypothesis that IL-15 and IL-2 share a common interface with IL-2R$\beta$ and $\gamma_c$, analysis of the IL-15 quaternary complex model shows that hA, hC, and hD adopt a similar conformation and that there are no major steric clashes between IL-15 and the IL-2R$\beta$/$\gamma_c$ receptors (Fig. 6*A*). Importantly, IL-15 residues Asp-8 in hA and Gln-108 in hD, which are conserved in IL-2 and known to be essential for IL-2R$\beta$ and $\gamma_c$ receptor binding, respectively (53), are positioned to make productive interactions (data not shown). The model also provides a likely explanation for the observation that Tyr-103 of $\gamma_c$ is more important for IL-15 binding than for IL-2 binding (54). In the IL-2 quaternary complex, Tyr-103 of $\gamma_c$ engages in hydrophobic contacts with IL-2 residues Gln-126, Ser-127, and the methyl group of Thr-123. Ser-127 of IL-2 has diverged to a methionine residue in IL-15 (Met-109) (Figs. 1*B* and 7), which substantially increases the hydrophobicity of this region and likely strengthens the interaction with Tyr-103 of $\gamma_c$. Sequence analysis shows that in addition to Asp-8 and Gln-108, many IL-15 residues at the predicted IL-15·IL-2R$\beta$/$\gamma_c$ interfaces are conserved or conservatively substituted (Fig. 1*B*), which likely imparts a degree of general binding affinity to IL-2 and IL-15 for the shared $\beta$ and $\gamma$ receptors. A notable difference observed in the IL-15 quaternary complex model at the IL-15·$\gamma_c$ interface is that an insertion of three residues and altered conformation of the hA–hB loop immediately preceding hB of IL-15 brings this region (IL-15 residues Asp-30, Phe-31, and His-32) in the vicinity of the hC–hC′1 loop of $\gamma_c$ (Fig. 7). Interestingly, the conformation of this loop region is stabilized by the unique disulfide bridge between Cys-35 in the hA–hB loop and Cys-85 in the hC–hD loop of IL-15. Potential contacts between IL-15 and the hC–hC′1 loop of $\gamma_c$ would be specific to IL-15, because this loop does not make contacts with IL-2 in the IL-2 quaternary complex. Overall the model is consistent with previous data showing that the $\beta$ and $\gamma_c$ receptors utilize an overlapping but non-identical binding surface for IL-2 and IL-15 and that there are differences in the relative contribution of individual residues to complex formation.

In contrast to formation of the IL-2 quaternary complex, which demonstrates cooperative binding ($K_d$ = 10–30 nM for IL-2·IL-2R$\alpha$; $K_d$ = 10 pM for IL-2 quaternary complex), there is not a significant increase in affinity of the IL-15 quaternary complex compared with the affinity of IL-15 for the $\alpha$ receptor alone ($K_d$ = 30–100 pM) (9, 12, 55). In the IL-2 quaternary complex, IL-2 residues Leu-12, Glu-15, Leu-18, and Leu-19 from the N-terminal portion of hA participate in interactions at a three-way junction between IL-2·IL-2R$\beta$ and $\gamma_c$ that is suggested to mediate cooperative binding (26). As mentioned above, one important difference between IL-2 and IL-15 is that hA of IL-15 is shorter by seven residues at its N terminus compared with IL-2 from the IL-2 receptor complex and is shorter by nine residues compared with IL-2 from the IL-2 quaternary complex (Figs. 1*B* and 7). Due to its shorter N terminus, in IL-15 there is no corresponding residue to Leu-12 of IL-2. In addition, residues Glu-15, Leu-18, and Leu-19 of IL-2 have diverged to Ile-3, Arg-6, and Tyr-7 in IL-15 (Figs. 1*B* and 7). It is tempting to suggest that, because of these differences in sequence and structure, the corresponding interactions at the IL-15·IL-2R$\beta$/$\gamma_c$ receptor junction cannot take place or are weakened in the IL-15 quaternary complex, which may partially account for the reduced cooperativity and stability of the IL-15 quaternary complex (6, 56). The precise details of the interactions at the IL-15·IL-2R$\beta$ and IL-15·$\gamma_c$ interfaces, and further insights into the molecular basis for the promiscuity of the IL-2R$\beta$ and $\gamma_c$ await the determination of the IL-15 quaternary complex structure.

Finally, there are data suggesting that human and mouse IL-15 exhibit some degree of species specificity in terms of signaling through IL-2Rβ/$\gamma_c$ (55). As mentioned above, comparison of our murine IL-15·IL-15Rα structure to the recently reported human IL-15·IL-15Rα structure (44) shows that the predicted IL-2Rβ and $\gamma_c$ binding sites of human and mouse IL-15 adopt a similar overall conformation. In contrast to mouse and human IL-15 residues involved in IL-15Rα binding, which are highly conserved, sequence analysis shows that there are several prominent amino acid substitutions at the predicted IL-2Rβ and $\gamma_c$ interfaces of mouse and human IL-15 (Fig. 1*B*). At the predicted $\gamma_c$ binding site, mouse IL-15 residues Arg-7, Glu-11, and Arg-105 have diverged to Ile-7, Arg-11, and His-105 in human IL-15, and at the predicted IL-2Rβ binding site, mouse Arg-64 has diverged to Glu-64 in human IL-15 (Fig. 1*B*). As mentioned above, the orientation of the alpha receptor binding site (hB) relative to that of the predicted IL-2Rβ/$\gamma_c$ binding site (hA, hC, and hD) is also slightly different in human and murine IL-15 (supplemental Figs. S1 and S2). Taken together, these sequence and structural differences may play some role in the observed species specificity for the ability IL-15 to signal through IL-15Rβ/$\gamma_c$ (55).

*Acknowledgments—We thank R. Akasaka for performing analytical ultracentrifugation, M. Hirafuji for MALDI-TOF and native gel analysis, A. Urushibata for DLS and N-terminal sequencing, T. Uchikubo-Kamo for assisting in protein crystallization, and N. Maoka, N. Ohbayashi, Y. Kinoshita-Sakaguchi, Y. Tomabechi, and S. Yokohata for cell-free protein synthesis. We also thank S. Tojo, N. Shinya, M. Ueno, T. Nagase, K. Honda, K. Usui, T. Inoue, and M. Aoki for cloning of expression constructs.*

## REFERENCES


1. Budagian, V., Bulanova, E., Paus, R., and Bulfone-Paus, S. (2006) *Cytokine Growth Factor Rev.* **17,** 259–280
2. Waldmann, T. A. (2006) *Nat. Rev. Immunol.* **6,** 595–601
3. Bamford, R. N., Grant, A. J., Burton, J. D., Peters, C., Kurys, G., Goldman, C. K., Brennan, J., Roessler, E., and Waldmann, T. A. (1994) *Proc. Natl. Acad. Sci. U. S. A.* **91,** 4940–4944
4. Grabstein, K. H., Eisenman, J., Shanebeck, K., Rauch, C., Srinivasan, S., Fung, V., Beers, C., Richardson, J., Schoenborn, M. A., Ahdieh, M., Johnson, L., Alderson, M. R., Watson, J. D., Anderson, D. M., and Giri, J. G. (1994) *Science* **264,** 965–968
5. Waldmann, T. A., Dubois, S., and Tagaya, Y. (2001) *Immunity* **14,** 105–110
6. Giri, J. G., Kumaki, S., Ahdieh, M., Friend, D. J., Loomis, A., Shanebeck, K., DuBose, R., Cosman, D., Park, L. S., and Anderson, D. M. (1995) *EMBO J.* **14,** 3654–3663
7. Dubois, S., Magrangeas, F., Lehours, P., Raher, S., Bernard, J., Boisteau, O., Leroy, S., Minvielle, S., Godard, A., and Jacques, Y. (1999) *J. Biol. Chem.* **274,** 26978–26984
8. Wei, X., Orchardson, M., Gracie, J. A., Leung, B. P., Gao, B., Guan, H., Niedbala, W., Paterson, G. K., McInnes, I. B., and Liew, F. Y. (2001) *J. Immunol.* **167,** 277–282
9. Giri, J. G., Ahdieh, M., Eisenman, J., Shanebeck, K., Grabstein, K., Kumaki, S., Namen, A., Park, L. S., Cosman, D., and Anderson, D. (1994) *EMBO J.* **13,** 2822–2830
10. Johnston, J. A., Bacon, C. M., Finbloom, D. S., Rees, R. C., Kaplan, D., Shibuya, K., Ortaldo, J. R., Gupta, S., Chen, Y. Q., Giri, J. D., and O'Shea, J. J. (1995) *Proc. Natl. Acad. Sci. U. S. A.* **92,** 8705–8709
11. Budagian, V., Bulanova, E., Orinska, Z., Ludwig, A., Rose-John, S., Saftig, P., Borden, E. C., and Bulfone-Paus, S. (2004) *J. Biol. Chem.* **279,** 40368–40375
12. Anderson, D. M., Kumaki, S., Ahdieh, M., Bertles, J., Tometsko, M., Loomis, A., Giri, J., Copeland, N. G., Gilbert, D. J., Jenkins, N. A., Valentine, V., Shapiro, D. N., Morris, S. W., Park, L. S., and Cosman, D. (1995) *J. Biol. Chem.* **270,** 29862–29869
13. Dubois, S., Mariner, J., Waldmann, T. A., and Tagaya, Y. (2002) *Immunity* **17,** 537–547
14. Leonard, W. J., Shores, E. W., and Love, P. E. (1995) *Immunol. Rev.* **148,** 97–114
15. Bernard, J., Harb, C., Mortier, E., Quemener, A., Meloen, R. H., Vermot-Desroches, C., Wijdeness, J., van Dijken, P., Grotzinger, J., Slootstra, J. W., Plet, A., and Jacques, Y. (2004) *J. Biol. Chem.* **279,** 24313–24322
16. Mortier, E., Quemener, A., Vusio, P., Lorenzen, I., Boublik, Y., Grotzinger, J., Plet, A., and Jacques, Y. (2006) *J. Biol. Chem.* **281,** 1612–1619
17. Myszka, D. G., Arulanantham, P. R., Sana, T., Wu, Z., Morton, T. A., and Ciardelli, T. L. (1996) *Protein Sci.* **5,** 2468–2478
18. Schluns, K. S., Stoklasek, T., and Lefrancois, L. (2005) *Int. J. Biochem. Cell Biol.* **37,** 1567–1571
19. Neely, G. G., Robbins, S. M., Amankwah, E. K., Epelman, S., Wong, H., Spurrell, J. C., Jandu, K. K., Zhu, W., Fogg, D. K., Brown, C. B., and Mody, C. H. (2001) *J. Immunol.* **167,** 5011–5017
20. Burkett, P. R., Koka, R., Chien, M., Chai, S., Boone, D. L., and Ma, A. (2004) *J. Exp. Med.* **200,** 825–834
21. Sandau, M. M., Schluns, K. S., Lefrancois, L., and Jameson, S. C. (2004) *J. Immunol.* **173,** 6537–6541
22. Sato, N., Patel, H. J., Waldmann, T. A., and Tagaya, Y. (2007) *Proc. Natl. Acad. Sci. U. S. A.* **104,** 588–593
23. Bulanova, E., Budagian, V., Duitman, E., Orinska, Z., Krause, H., Ruckert, R., Reiling, N., and Bulfone-Paus, S. (2007) *J. Biol. Chem.* **282,** 13167–13179
24. Kobayashi, H., Dubois, S., Sato, N., Sabzevari, H., Sakai, Y., Waldmann, T. A., and Tagaya, Y. (2005) *Blood* **105,** 721–727
25. Wang, X., Rickert, M., and Garcia, K. C. (2005) *Science* **310,** 1159–1163
26. Stauber, D. J., Debler, E. W., Horton, P. A., Smith, K. A., and Wilson, I. A. (2006) *Proc. Natl. Acad. Sci. U. S. A.* **103,** 2788–2793
27. Lorenzen, I., Dingley, A. J., Jacques, Y., and Grotzinger, J. (2006) *J. Biol. Chem.* **281,** 6642–6647
28. Quemener, A., Bernard, J., Mortier, E., Plet, A., Jacques, Y., and Tran, V. (2006) *Proteins* **65,** 623–636
29. Rubinstein, M. P., Kovar, M., Purton, J. F., Cho, J. H., Boyman, O., Surh, C. D., and Sprent, J. (2006) *Proc. Natl. Acad. Sci. U. S. A.* **103,** 9166–9171
30. Kigawa, T., Yamaguchi-Nunokawa, E., Kodama, K., Matsuda, T., Yabuki, T., Matsuda, N., Ishitani, R., Nureki, O., and Yokoyama, S. (2002) *J. Struct. Funct. Genomics* **2,** 29–35
31. Otwinowski, Z., and Minor, W. (1997) *Methods Enzymol.* **276,** 307–326
32. Terwilliger, T. C., and Berendzen, J. (1999) *Acta Crystallogr. D. Biol. Crystallogr.* **55,** 849–861
33. Terwilliger, T. C. (2000) *Acta Crystallogr. D. Biol. Crystallogr.* **56,** 965–972
34. Perrakis, A., Morris, R., and Lamzin, V. S. (1999) *Nat. Struct. Biol.* **6,** 458–463
35. Brunger, A. T., Adams, P. D., Clore, G. M., DeLano, W. L., Gros, P., Grosse-Kunstleve, R. W., Jiang, J. S., Kuszewski, J., Nilges, M., Pannu, N. S., Read, R. J., Rice, L. M., Simonson, T., and Warren, G. L. (1998) *Acta Crystallogr. D. Biol. Crystallogr.* **54,** 905–921
36. Jones, T. A., Zou, J. Y., Cowan, S. W., and Kjeldgaard, G. (1991) *Acta Crystallogr. A.* **47,** 110–119
37. Laskowski, R. A., MacArthur, M. W., Moss, D. S., and Thornton, J. M. (1993) *J. Appl. Cryst.* **26,** 283–291
38. Potterton, L., McNicholas, S., Krissinel, E., Gruber, J., Cowtan, K., Emsley, P., Murshudov, G. N., Cohen, S., Perrakis, A., and Noble, M. (2004) *Acta Crystallogr. D. Biol. Crystallogr.* **60,** 2288–2294
39. Dexter, T. M., Garland, J., Scott, D., Scolnick, E., and Metcalf, D. (1980) *J. Exp. Med.* **152,** 1036–1047
40. Ruchatz, H., Leung, B. P., Wei, X. Q., McInnes, I. B., and Liew, F. Y. (1998) *J. Immunol.* **160,** 5654–5660
41. Rozwarski, D. A., Gronenborn, A. M., Clore, G. M., Bazan, J. F., Bohm, A., Wlodawer, A., Hatada, M., and Karplus, P. A. (1994) *Structure* **2,** 159–173
42. Rickert, M., Wang, X., Boulanger, M. J., Goriatcheva, N., and Garcia, K. C.

(2005) *Science* **308,** 1477–1480
43. Norman, D. G., Barlow, P. N., Baron, M., Day, A. J., Sim, R. B., and Campbell, I. D. (1991) *J. Mol. Biol.* **219,** 717–725
44. Chirifu, M., Hayashi, C., Nakamura, T., Toma, S., Shuto, T., Kai, H., Yamagata, Y., Davis, S. J., and Ikemizu, S. (2007) *Nat. Immunol.* **8,** 1001–1007
45. de Vos, A. M., Ultsch, M., and Kossiakoff, A. A. (1992) *Science* **255,** 306–312
46. Aritomi, M., Kunishima, N., Okamoto, T., Kuroki, R., Ota, Y., and Morikawa, K. (1999) *Nature* **401,** 713–717
47. Hage, T., Sebald, W., and Reinemer, P. (1999) *Cell* **97,** 271–281
48. Yoon, C., Johnston, S. C., Tang, J., Stahl, M., Tobin, J. F., and Somers, W. S. (2000) *EMBO J.* **19,** 3530–3541
49. Stoklasek, T. A., Schluns, K. S., and Lefrancois, L. (2006) *J. Immunol.* **177,** 6072–6080
50. Liparoto, S. F., and Ciardelli, T. L. (1999) *J. Mol. Recognit.* **12,** 316–321
51. Olosz, F., and Malek, T. R. (2000) *J. Biol. Chem.* **275,** 30100–30105
52. Bulanova, E., Budagian, V., Orinska, Z., Krause, H., Paus, R., and Bulfone-Paus, S. (2003) *J. Immunol.* **170,** 5045–5055
53. Pettit, D. K., Bonnert, T. P., Eisenman, J., Srinivasan, S., Paxton, R., Beers, C., Lynch, D., Miller, B., Yost, J., Grabstein, K. H., and Gombotz, W. R. (1997) *J. Biol. Chem.* **272,** 2312–2318
54. Olosz, F., and Malek, T. R. (2002) *J. Biol. Chem.* **277,** 12047–12052
55. Eisenman, J., Ahdieh, M., Beers, C., Brasel, K., Kennedy, M. K., Le, T., Bonnert, T. P., Paxton, R. J., and Park, L. S. (2002) *Cytokine* **20,** 121-129
56. de Jong, J. L., Farner, N. L., Widmer, M. B., Giri, J. G., and Sondel, P. M. (1996) *J. Immunol.* **156,** 1339–1348